High-pressure study of $ScVO_4$ by Raman scattering and *ab initio* calculations

V. Panchal,[1] F. J. Manjón,[2] D. Errandonea,[1,*] P. Rodriguez-Hernandez,[3] J. López-Solano,[3] A. Muñoz,[3] S. N. Achary,[4] and A. K. Tyagi[4]

[1]*Departamento de Física Aplicada—ICMUV, Universidad de Valencia, Edificio de Investigación, C/Dr. Moliner 50, 46100 Burjassot (Valencia), Spain*

[2]*Instituto de Diseño para la Fabricación y Producción Automatizada, Universidad Politécnica de Valencia, Camino de Vera s/n, 46022 Valencia, Spain*

[3]*Departamento de Física Fundamental II, Instituto de Materiales y Nanotecnología, Universidad de La Laguna, La Laguna 38205, Tenerife, Spain*

[4]*Chemistry Division, Bhabha Atomic Research Center, Trombay, Mumbai 400085, India*

(Received 29 October 2010; revised manuscript received 3 January 2011; published 25 February 2011)

We report results of experimental and theoretical lattice-dynamics studies on scandium orthovanadate up to 35 GPa. Raman-active modes of the low-pressure zircon phase are measured up to 8.2 GPa, where the onset of an irreversible zircon-to-scheelite phase transition is detected. Raman-active modes in the scheelite structure are observed up to 16.5 GPa. Beyond 18.2 GPa we detected a gradual splitting of the E_g modes of the scheelite phase, indicating the onset of a second phase transition. Raman symmetries, frequencies, and pressure coefficients in the three phases of $ScVO_4$ are discussed in the light of *ab initio* lattice-dynamics calculations that support the experimental results. The results on all the three phases of $ScVO_4$ are compared with those previously reported for related orthovanadates.

DOI: 10.1103/PhysRevB.83.064111 PACS number(s): 62.50.−p, 63.20.−e, 78.30.−j, 71.15.Mb

I. INTRODUCTION

Orthovanadates with composition AVO_4 (A = trivalent metal) with pentavalent vanadium are found in numerous applications due to their interesting magnetic, optical, and electronic properties. In addition to their wide practical applicability, these materials are also commonly used as cathodoluminescent materials, thermophosphors, scintillators, photocatalysis materials, and in lithium ion batteries.[1,2] As a consequence of the many applications of orthovanadates in recent years they have been extensively investigated under high pressure (HP), like other ABO_4 compounds, in order to understand their mechanical properties and HP structural phase transitions.[3]

$ScVO_4$ crystallizes in the tetragonal zircon-type structure (space group $I4_1/amd$, $Z = 2$) at ambient conditions. In this structure, the vanadium atom is tetrahedrally coordinated while the trivalent metal is coordinated to eight oxygen atoms.[4] Recent x-ray diffraction (XRD) measurements on $ScVO_4$ have shown the onset of a nonreversible structural phase transition from the low-pressure zircon-type structure to a denser scheelite-type structure (space group $I4_1/a$, $Z = 4$) at 8.7 GPa.[5] *Ab initio* calculations confirmed this transition (at 5.8 GPa) and predicted the existence of a second one at 9 GPa.[6] In contrast, XRD measurements found the scheelite-type structure to be stable up to 27 GPa. In this respect, we have to note that similar discrepancies were observed earlier in isomorphic YVO_4. They were resolved by the combination of HP Raman measurements and lattice-dynamics calculations.[7] In that paper it was shown that YVO_4 undergoes a phase transition from the zircon to the scheelite structure at 7.5 GPa in agreement with previous XRD data[8] and a second phase transition above 20 GPa toward a fergusonite phase which was predicted by total-energy *ab initio* calculations but was not clearly observed in XRD measurements until 26 GPa.[8] To the best of our knowledge, there is no HP Raman study of $ScVO_4$ reported yet. Here, we report Raman scattering measurements in $ScVO_4$ up to 35 GPa together with *ab initio* lattice-dynamics calculations. Our purpose is to assign the symmetry of the Raman modes in the zircon and scheelite phases of $ScVO_4$ and to explore the possible scheelite-to-fergusonite transition as theoretically predicted. Further, we will compare and discuss the results on $ScVO_4$ with those of other orthovanadates and orthophosphates.

II. EXPERIMENTAL DETAILS

$ScVO_4$ samples used in the experiments were prepared by solid state reaction of appropriate amounts of predried Sc_2O_3 (Indian Rare Earth Ltd., 99%) and V_2O_5 (Alfa-Aesar, 99%). Homogeneous mixtures of the reactants were pelletized and heated at 800 °C for 24 h and then cooled to room temperature. Further, the pellets were reground and heated again at 1100 °C for 24 h. The sample obtained was characterized by powder x-ray diffraction recorded on a Philips X-pert Pro diffractometer using Cu $K\alpha$ radiation. A single phase of $ScVO_4$ of zircon-type structure was confirmed with structural parameters identical to those reported in Ref. 5.

The prepared powder sample of $ScVO_4$, along with a 2-μm-diameter ruby ball, was loaded in a preindented steel gasket with a 200-μm-diameter hole inside a diamond-anvil cell. A 4:1 methanol-ethanol mixture was used as pressure-transmitting medium.[9,10] The pressure was determined by monitoring the shift in ruby fluorescence lines.[11] HP Raman measurements were performed in the backscattering geometry using a 632.8 nm HeNe laser and a Horiba Jobin Yvon LabRAM HR UV microspectrometer in combination with a thermoelectric-cooled multichannel CCD detector with spectral resolution below 2 cm^{-1}. Three experimental runs were carried out with similar results.

III. LATTICE-DYNAMICS CALCULATIONS

The calculations reported here have been performed using the formalism of density-functional theory. In particular, the Vienna simulation package VASP (see Refs. 12 and 13 and references therein) has been used to perform structural calculations with the pseudopotential method. The set of plane waves employed extended up to a kinetic energy cutoff of 540 eV; such a large cutoff was required to achieve highly converged results within the projector augmented wave (PAW) scheme.[14,15] The PAW method takes into account the full nodal character of all the electron charge-density distribution in the core region. The exchange-correlation energy was initially taken in the generalized-gradient approximation with the Perdew-Burke-Ernzerhof prescription.[16] We used a dense grid of k-special points for integrations along the Brillouin zone (BZ) in order to assure highly converged results to about 1–2 meV per formula unit, yielding accurate and well-converged forces. At each selected volume, the structures were fully relaxed to their equilibrium configuration through the calculation of the forces on atoms and the stress tensor.[17] In the relaxed equilibrium configuration, the forces are less than 0.004 eV/Å and the deviation of the stress tensor from a diagonal hydrostatic form is less than 0.2 GPa. Lattice-dynamics calculations of phonon modes were performed in zircon, scheelite, and fergusonite structures at the zone center (Γ point) of the BZ. The calculations provided information about the frequency, symmetry, and polarization vector of the vibrational modes in each structure. Highly converged results on forces are required for the calculation of the dynamical matrix of lattice-dynamics calculations. We use the direct force-constant approach (or supercell method).[18] The construction of the dynamical matrix at the Γ point of the BZ is particularly simple and involves separate calculation of the forces in which a fixed displacement from the equilibrium configuration of the atoms within the primitive unit cell is considered. Symmetry further reduces the computational efforts by reducing the number of such independent displacements in the analyzed structures. Diagonalization of the dynamical matrix provides both the frequencies of the normal modes and their polarization vectors. It allows us to identify the irreducible representations and the character of phonon modes at the Γ point.

IV. RESULTS

A. Zircon-structured $ScVO_4$

At ambient conditions, $ScVO_4$ exists in the zircon structure (space group $I4_1/amd$, point group D_{4h}) with two formula units per primitive cell. The BO_4 units are the building blocks of the tetragonal zircon structure of ABO_4 compounds. Therefore, the vibrational modes of the ABO_4 compounds can be classified as either internal or external modes of the BO_4 unit. The external modes correspond either to a pure translation (T) or to a pure rotation (R) of the BO_4 molecule; while the internal modes can be decomposed into four types of motion (ν_1, ν_2, ν_3, and ν_4) in view of the T_d symmetry of the BO_4 molecule.[19] The reduction of the representation of T_d symmetry under the D_{2d} symmetry of the VO_4 site in the zircon lattice of $ScVO_4$ and the transformation of the D_{2d} representation to the D_{4h} representation yields 12 first-order Raman-active modes at the center of the BZ with symmetries $\Gamma = 2A_{1g} + 4B_{1g} + B_{2g} + 5E_g$,[20] whose classification into internal and external modes yields

$$\Gamma = A_{1g}(\nu_1,\nu_2) + B_{1g}(2T,\nu_3,\nu_4) + B_{2g}(\nu_2) + E_g(2T,R,\nu_3,\nu_4). \quad (1)$$

Figure 1(a) shows the Raman spectra of $ScVO_4$ in the zircon phase at different pressures up to 7.6 GPa. The Raman spectrum in orthovanadates can be divided into two regions.[7,20,21] The high-frequency region (800–950 cm^{-1}) comprises the region where the symmetric stretching mode $\nu_1(A_{1g})$ and the asymmetric stretching modes $\nu_3(E_g)$ and $\nu_3(B_g)$ are observed. The low-frequency region (250–500 cm^{-1}) comprises the region of the bending modes. At ambient conditions 10 out of the 12 first-order Raman peaks are clearly discernable. Apart from these first-order Raman modes we have observed three additional peaks in the frequency gap of 500–800 cm^{-1} [marked by asterisks in Fig. 1(a)]. They are likely to be second-order Raman modes. The symmetry assignment for the first-order modes has been performed in accordance with our calculations and comparison with previous results in other vanadates and it is summarized in Table I.

Regarding the analysis of the Raman spectra of the zircon phase, it can be noted that the intense symmetric stretching internal mode $\nu_1(A_{1g})$, observed at 914 cm^{-1} at ambient pressure (10^{-4} GPa), is the highest in frequency among the family of orthovanadates.[22] This indicates that $ScVO_4$ exhibits the strongest intratetrahedral V-O bonds among orthovanadates. Apart from this mode, we have observed two asymmetric stretching modes $\nu_3(E_g)$ and $\nu_3(B_{1g})$ at 826 and 817 cm^{-1}, respectively. Note that in $ScVO_4$, as in other vanadates,[5,22] ν_1 has a higher frequency than ν_3. However, this relation becomes opposite (i.e., $\nu_1 < \nu_3$) in $ScPO_4$.[23] This difference is due to the increase in covalence on the V-O bond resulting from the

TABLE I. *Ab initio* calculated and experimental frequencies at ambient conditions, pressure coefficients, and mode Grüneisen parameters of $ScVO_4$ in the zircon phase. The mode Grüneisen parameter was obtained from $\gamma = (B_0/\omega_0)d\omega/dP$. The bulk modulus $B_0 = 178$ GPa is taken from Ref. 5.

Raman mode symmetry	ω_0[a] (cm^{-1})	$\frac{d\omega}{dp}$[a] (cm^{-1}/GPa)	ω_0[b] (cm^{-1})	$\frac{d\omega}{dp}$[b] (cm^{-1}/GPa)	γ[b]
$T(E_g)$	109.3	1.01	119.3	0.89	1.33
$T(E_g)$	159.5	−0.18	165.6	−0.05	−0.05
$T(B_{1g})$	163.2	3.72	180.5	2.42	2.39
$\nu_2(B_{2g})$	255.6	−1.37	263.2	−1.15	−0.78
$T(B_{1g})$	263.2	2.68	–	–	–
$R(E_g)$	281.6	6.69	304.8	6.28	3.67
$\nu_2(A_{1g})$	326.5	2.15	356.7	2.06	0.94
$\nu_4(E_g)$	377.7	0.82	–	–	–
$\nu_4(B_{1g})$	462.5	2.39	494.1	2.62	0.94
$\nu_3(B_{1g})$	827.6	5.78	817.1	5.79	1.26
$\nu_3(E_g)$	848.7	5.78	856.5	5.31	1.10
$\nu_1(A_{1g})$	905.6	5.33	914.2	5.61	1.09

[a]Theoretical calculations.
[b]Experimental data.

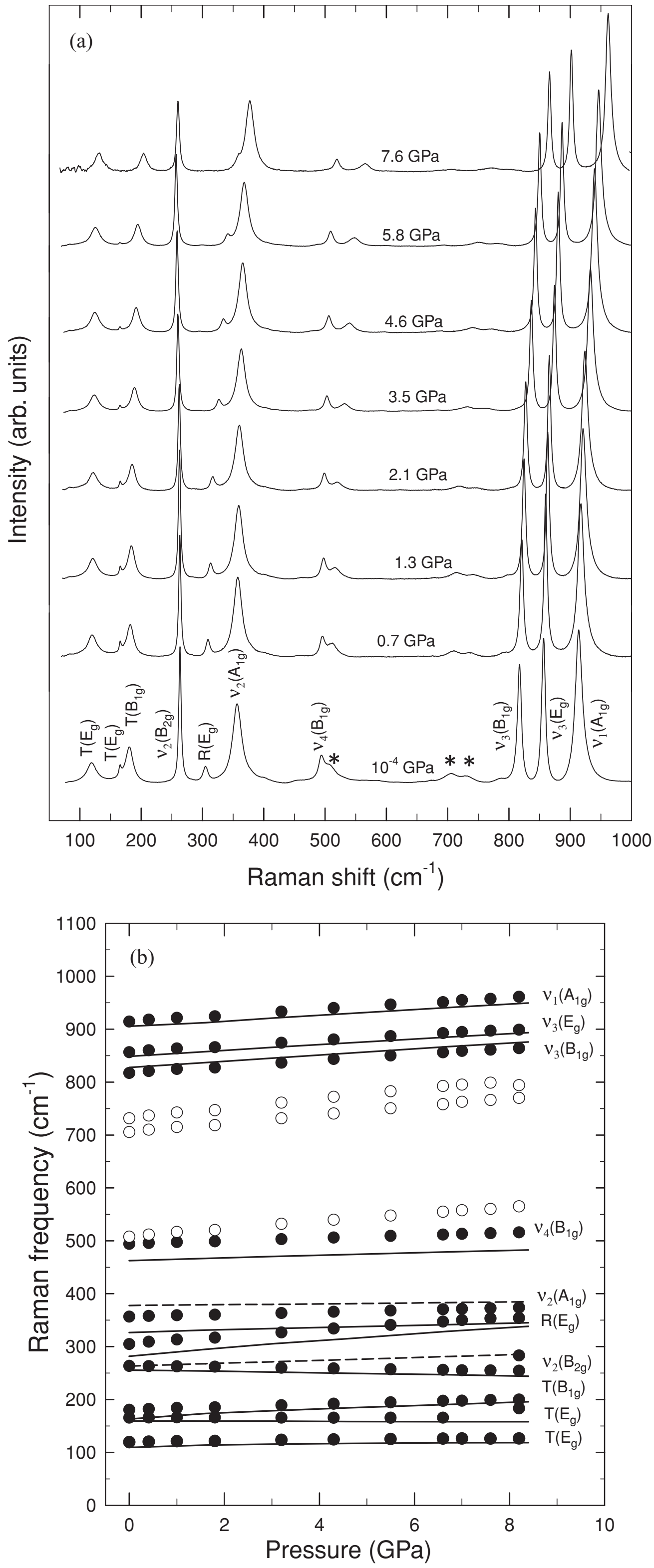

FIG. 1. (a) Raman spectra of $ScVO_4$ in the zircon phase between 1 atm and 7.6 GPa. Asterisks represent the second-order Raman modes. (b) Pressure dependence of the Raman mode frequencies in zircon-type $ScVO_4$ (solid symbols). Empty symbols are likely second-order Raman modes. Th solid lines are the calculated modes. The dashed lines represent Raman modes not observed in the experiments.

shift of the energies of the V 3d states relative to the O 2p valence band.[24] Regarding the other phonons of $ScVO_4$, out of four bending modes of the VO_4 unit we could observe only three: $\nu_4(B_{1g})$ at 494 cm^{-1}, $\nu_2(A_{1g})$ at 356 cm^{-1}, and $\nu_2(B_{2g})$ at 263 cm^{-1}. The asymmetric bending mode $\nu_4(E_g)$ could not be detected. Similarly, one of the external translational $T(B_{1g})$ modes has not been detected. In most of the Raman measurements in orthovanadates these two modes are absent, probably due to their weak Raman scattering cross section.[22]

Figure 1(b) shows the pressure dependence of Raman modes in the zircon phase. The symmetry assignment for the Raman modes along with their experimental and calculated frequencies, pressure coefficients, and mode Grüneisen parameters (γ) are shown in Table I. Agreement between experimental and calculated frequencies and pressure coefficients for the Raman modes is rather good. The Grüneisen parameters of the different modes in the zircon phase have been obtained by using the bulk modulus $B_0 = 178$ GPa reported earlier by XRD measurements on $ScVO_4$.[5]

The frequencies of the Raman modes of the zircon phase were found to increase with increasing pressure except for the external $T(E_g)$ mode at 165 cm^{-1} and the internal $\nu_2(B_{2g})$ mode at 263 cm^{-1} at ambient pressure, which exhibit negative pressure coefficients. A similar behavior was observed for other orthovanadates, e.g., YVO_4,[7] $YbVO_4$,[21] and $LuVO_4$,[25] and also in $ScPO_4$.[23] This softening of the two modes seems to be a characteristic behavior of zircon-type compounds. The pressure coefficient of the $\nu_2(B_{2g})$ bending mode, assigned in other works as the $T(E_g)$ or $T(B_g)$ mode, is found to be similar among orthovanadates and of the order of -1.2 to -1.4 cm^{-1}/GPa.[7,21,25,26] On the other hand, the pressure coefficient of the $T(E_g)$ mode with the lowest frequency is very small (-0.05 cm^{-1}/GPa) for $ScVO_4$ and is similar in the case of YVO_4,[7] while it is slightly larger for other compounds.[21,25] Softening of $T(E_g)$ and $\nu_2(B_{2g})$ modes in zircon-type compounds evidences an induced distortion in the zircon structure responsible for the instability of this phase. This has been observed not only when zircon transforms to scheelite, but also when it transforms to other structures like monazite, an intermediate phase in YPO_4.[23] In fact, phonon softening indicates that the translational motions of Sc and V atoms increase while approaching a dynamical instability of zircon at high pressure. In particular, we consider that the softening of the external $T(E_g)$ mode, in which the VO_4 tetrahedra vibrate in the plane perpendicular to the c-axis, can be considered as indicative of the zircon-to-scheelite phase transition upon compression.[7,21,25,26] Recently, two transformation mechanisms were suggested for the zircon-scheelite transition.[27,28] In both studies the elastic shear strain was assumed as the main factor driving the transformation. The phonon softening we observed is consistent with this argument but we cannot discriminate between the proposed transition mechanisms. A detailed study of them is beyond the scope of this work.

In general, we have found very similar pressure coefficients for the Raman mode frequencies in orthovanadates; e.g., the pressure coefficients for the internal stretching modes and the highest-frequency $T(E_g)$ mode are found to be of the order of 5.2 to 6.4 cm^{-1}/GPa. To close this description of the pressure evolution of Raman phonons we would like to add that the rotational $R(E_g)$ mode of $ScVO_4$ has the largest pressure coefficient (see Table I). The same large pressure coefficient is observed for this mode in $ScPO_4$,[23] and indicates a strengthening of the Sc-VO_4 bonds with compression. This result suggests that the small Sc^{3+} cation leads to a tension of VO_4 units in the zircon phase that does not favor the rotation of the VO_4 units around the *c*-axis. Furthermore, on increasing pressure the decrease of the Sc^{3+} ionic radius makes this effect even stronger. On the contrary, zircon-type AVO_4 compounds with an A cation with larger ionic radius than Sc, like rare earths, would tend to facilitate the rotation of the VO_4 units, leading to smaller pressure coefficients for the rotational mode.

B. Scheelite-structured $ScVO_4$

As already mentioned, recent XRD measurements in $ScVO_4$ show that it undergoes a zircon-to-scheelite phase transition around 8.7 GPa.[5] This value is somewhat higher than that obtained from theoretical calculations (5.8 GPa).[6] Group theoretical calculations for $ScVO_4$ in the scheelite phase (space group $I4_1/a$, point group C_{4h}^6) predict 13 first-order Raman modes at the BZ center with the symmetries $\Gamma = 3A_g + 5B_g + 5E_g$.[29] These modes can be further classified as either internal (ν_1 to ν_4) or external (T and R) modes of the VO_4 units,

$$\Gamma = \nu_1(A_g) + \nu_2(A_g) + \nu_2(B_g) + \nu_3(B_g) + \nu_3(E_g) + \nu_4(B_g) + \nu_4(E_g) + R(A_g) + R(E_g) + 2T(B_g) + 2T(E_g). \quad (2)$$

Raman spectra of $ScVO_4$ in the scheelite phase are shown in Figure 2(a). Around 8.2 GPa we have observed the appearance of two extra Raman bands at 183 and 283 cm^{-1}; these two modes are assigned as $T(E_g)$, and $\nu_2(A_g)$ modes of the scheelite phase, indicating the onset of the zircon-to-scheelite phase transition. At higher pressures, we observed the appearance of many Raman bands, as shown by arrows in Fig. 2(a), accompanied by broadening of the Raman modes. A weak presence of the Raman modes of the zircon phase can be detected up to 15.1 GPa. The coexistence of the low- and high-pressure phases is consistent with XRD studies.[5] A typical feature of the transition is that the frequency of the symmetric stretching mode $\nu_1(A_g)$ drops abruptly across it. These changes in the Raman spectra are indicative of a structural phase transition toward the lower-symmetry tetragonal scheelite phase, as already observed in other orthovanadates.[7,21,25,26] Out of 13 Raman-active modes in the scheelite phase, we observed only 11 modes with measurable intensity up to 16.5 GPa. Above this pressure, changes in the Raman spectra point toward a possible second phase transition which will be discussed in the next section.

The mode assignment of the experimentally observed Raman modes in $ScVO_4$ in the scheelite phase was done according to our calculations and is shown in Table II. The highest-frequency mode at 826 cm^{-1} is assigned to the symmetric stretching mode $\nu_1(A_g)$ and its frequency is observed to be approximately similar in the scheelite phase of other orthovanadates, like YVO_4, $YbVO_4$, $DyVO_4$, and $TbVO_4$, irrespective of the V-O bond distance.[7,21,26] This behavior is completely different from that observed in the

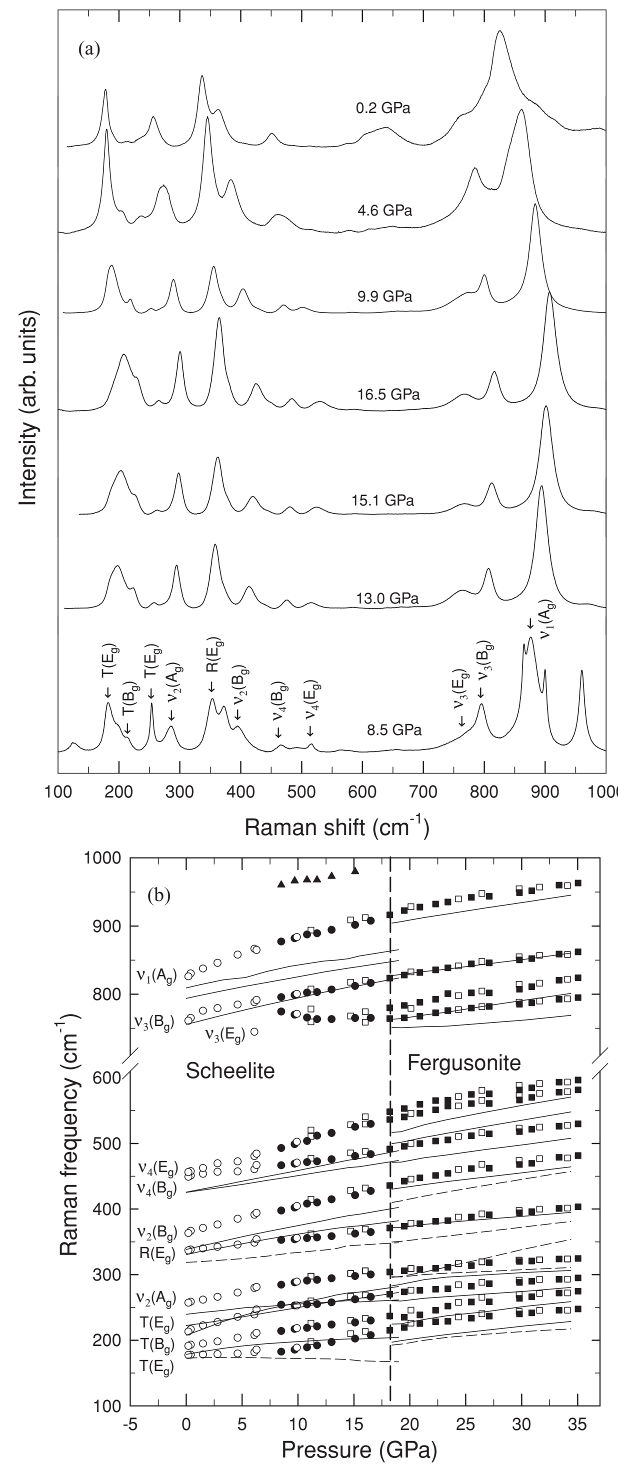

FIG. 2. (a) Raman spectra of the scheelite phase of $ScVO_4$ at pressures between 8.5 and 16.5 GPa on the upstroke and between 9.9 and 0.2 GPa on the downstroke. (b) Experimental pressure dependence of the Raman mode frequencies in scheelite- and fergusonite-type $ScVO_4$. Filled and empty circles correspond to Raman modes in scheelite-type $ScVO_4$ during the upstroke and downstroke, respectively. Filled and empty squares correspond to Raman modes in fergusonite-type $ScVO_4$ on the upstroke and downstroke, respectively. Filled triangles are likely second-order modes of the scheelite phase. The solid lines are the calculated modes. The dashed lines represent Raman modes not observed in the experiments.

TABLE II. *Ab initio* calculated and experimental frequencies at ambient conditions, pressure coefficients, and mode Grüneisen parameters of $ScVO_4$ in the scheelite phase. The mode Grüneisen parameter was obtained from $\gamma = (B_0/\omega_0)d\omega/dP$. The bulk modulus $B_0 = 210$ GPa is taken from Ref. 5.

Raman mode symmetry	ω_0[a] (cm^{-1})	$\frac{d\omega}{dp}$[a] (cm^{-1}/GPa)	ω_0[b] (cm^{-1})	$\frac{d\omega}{dp}$[b] (cm^{-1}/GPa)	γ[b]
$T(B_g)$	172.8	−0.19	–	–	–
$T(E_g)$	178.5	1.56	177.5	3.18	3.76
$T(B_g)$	207.8	3.51	191.3	1.96	2.15
$T(E_g)$	222.5	2.84	213.1	1.62	1.59
$\nu_2(A_g)$	239.6	2.17	257.0	1.87	1.53
$R(A_g)$	318.7	1.71	–	–	–
$R(E_g)$	330.4	2.92	336.0	1.55	0.97
$\nu_2(B_g)$	338.2	3.52	363.2	3.62	2.09
$\nu_4(B_g)$	425.3	2.62	449.0	2.11	0.99
$\nu_4(E_g)$	425.7	3.35	456.0	4.68	2.16
$\nu_3(E_g)$	755.8	3.75	727.5	0.41	0.12
$\nu_3(B_g)$	793.9	3.05	760.9	2.53	0.69
$\nu_1(A_g)$	809.3	3.42	826.1	3.72	0.95

[a]Theoretical calculations.
[b]Experimental data.

zircon phase, where the highest-frequency mode scales with the V-O bond distance in the different vanadates. The different behaviors of the symmetric stretching modes in zircon and scheelite phases will be addressed in Sec. V. The other two asymmetric stretching modes of the scheelite phase of $ScVO_4$ are observed near 760 and 726 cm^{-1} and assigned to $\nu_3(E_g)$ and $\nu_3(B_g)$ modes, respectively. The four bending vibrations are observed experimentally at 456, 449, 363, and 257 cm^{-1} and assigned to the $\nu_4(E_g)$, $\nu_4(B_g)$, $\nu_2(B_g)$, and $\nu_2(A_g)$ modes, respectively. Additionally, we could observe four out six external modes predicted for the scheelite phase up to the highest pressure attained in our experiment [see Fig. 2(a)]. The external translational mode of $T(B_g)$ symmetry with the lowest frequency could not be detected, likely due to its weak intensity and the fact that, according to our calculations, it is very close to the intense $T(E_g)$ mode. Curiously, our calculations predicted the softening of this $T(B_g)$ mode, which we have not been able to measure. Similarly, the rotational $R(A_g)$ mode, derived from the silent rotational $R(A_g)$ mode of the zircon phase, could not be detected due to its weak intensity. In general, the calculated Raman frequencies are in good agreement with our experimental frequencies with maximum deviation of 7.5%. The same agreement of experiment and calculations holds for the Raman frequency pressure coefficients. All these data are shown in Table II together with mode Grüneisen parameters (γ), calculated using the bulk modulus of the scheelite phase, $B_0 = 210$ GPa, as reported in Ref. 5.

Figure 2(b) shows the pressure evolution of the Raman modes of $ScVO_4$ in the scheelite phase. As mentioned earlier, our calculations indicate the softening of the external $T(B_g)$ mode of the lowest frequency in the scheelite phase with increasing pressure with a very small pressure coefficient (−0.19 cm^{-1}/GPa). A similar softening of this $T(B_g)$ mode was predicted by lattice-dynamics calculations and indeed experimentally found in YVO_4.[7] However, the softening of the lowest-frequency $T(B_g)$ Raman mode has not been reported in the studies published on $YbVO_4$,[21] $LuVO_4$,[25,30] $TbVO_4$, and $DyVO_4$.[26] Curiously, a similar softening of the lowest-frequency $T(B_g)$ mode is frequently observed in the family of scheelite tungstates and molybdates that undergo a scheelite-to-fergusonite transition.[31–33]

From the knowledge of stretching mode frequencies of orthovanadates we can estimate the Pauling bond strength, also referred to as the bond valence, of V-O bonds. The general relation between stretching mode frequency and bond length R (in Å) in the vanadium oxides is given as[34]

$$\omega(cm^{-1}) = 21349\exp(-1.9176R). \quad (3)$$

There exists a relationship between the bond length R (Å) and the Pauling bond strength S, which is given by[35]

$$S_{V-O} = (R/1.791)^{-5.1}. \quad (4)$$

Here, S_{V-O} is expressed in valence units (v.u.), and one valence unit corresponds to 1.791 Å in bond length. The observed stretching frequencies of VO_4 units in the zircon phase of $ScVO_4$ at ambient pressure are 914.2, 856.5, and 817.1 cm^{-1}. The corresponding bond lengths using Eq. (3) are 1.64, 1.68, and 1.70 Å, and the three bond strengths using Eq. (4) are 1.55, 1.39, and 1.29 v.u., respectively. Adding these bond strengths by counting twice the contribution from the shortest bond length on account of the fourfold coordination in VO_4 we can estimate the total valence as 5.52 v.u., which is close to but higher than the valence of the V^{5+} ion. A similar overestimation of the total valence of V in the zircon phase was also recently found for YVO_4.[7]

Similarly, we can estimate the Pauling bond strength of $ScVO_4$ in the scheelite phase by taking into account the stretching-mode frequencies. The observed stretching-mode frequencies in the scheelite phase of $ScVO_4$ at ambient pressure are 826.1, 760.9, and 727.5 cm^{-1}. The corresponding bond lengths using Eq. (3) are 1.70, 1.74, and 1.76 Å, and the three corresponding bond strengths obtained by using Eq. (4) are 1.31, 1.16, and 1.09 v.u., respectively. Summing these bond strengths by counting twice the contribution from the shortest bond length on account of the fourfold coordination in VO_4 we can estimate a total valence of 4.65 v.u., which is close to the valence of the V^{5+} ion. A similar value for the total valence of the V^{5+} ion was obtained for YVO_4 at ambient pressure in Ref. 7. The value of the bond strength in the scheelite phase is quite small as compared to the zircon phase (5.52 v.u. at ambient pressure). Since the bond strength should be around 5, and taking into account that it increases with increasing pressure, we can consider that the scheelite phase of $ScVO_4$ is a very stable phase while the high value of the bond strength in the zircon phase could be indicative of the instability of the zircon phase of $ScVO_4$. The same conclusions were drawn in Ref. 7 for YVO_4 and give support to the metastability of the scheelite phase observed at ambient pressure in many zircon-type compounds on the downstroke. In this sense, Fig. 2(a) shows the Raman spectra of $ScVO_4$ on the downstroke from 16.5 GPa to ambient pressure. It can be observed that on release of pressure the scheelite phase does not revert back to the zircon phase, thus evidencing the irreversible nature of the zircon-to-scheelite phase transition and the metastable character of the scheelite phase at ambient conditions.

C. Fergusonite-structured $ScVO_4$

As already commented, a scheelite-to-fergusonite phase transition has been observed in a number of orthovanadates, and our theoretical calculations for $ScVO_4$ suggest a scheelite-to-fergusonite phase transition above 9 GPa.[6] Group theoretical calculations for $ScVO_4$ in the fergusonite phase (space group $I2/a$, point group C_{2h}^6) predict 18 first-order Raman modes near the BZ center with the symmetries $\Gamma = 8A_g + 10B_g$. The correlation between the scheelite and fergusonite Raman modes is as follows: every A_g and B_g scheelite mode converts into an A_g mode of monoclinic symmetry while every doubly degenerate E_g mode converts into two B_g modes.

Figure 3 shows the Raman spectra of $ScVO_4$ from 16.5 to 35 GPa. Beyond 18.2 GPa we have observed noticeable changes in the Raman spectra. In particular, both the $\nu_3(E_g)$ mode at 540 cm^{-1} and $\nu_4(E_g)$ mode at 770 cm^{-1} (marked with arrows in Fig. 3) of scheelite-type $ScVO_4$ show a considerable broadening. We have interpreted these broadenings as associated with the splitting of E_g modes into two B_g modes in the fergusonite phase beyond 18.2 GPa (see arrows in Fig. 3). Raman measurements in the orthovanadates YVO_4, $YbVO_4$, and $LuVO_4$ also report such splitting of E_g modes,[7,21,25] and the same holds for the scheelite tungstates $BaWO_4$ and $PbWO_4$.[31,32] Furthermore, lattice-dynamics calculations for the fergusonite phase are in good agreement with the experimental results. The splitting of E_g modes could only be observed for the V-O stretching modes. Among the external E_g modes the splitting could not be detected. A similar behavior was observed in the cases of $YbVO_4$ and $LuVO_4$.[21,25] Hence, to fully understand the observed changes in the Raman spectra at 18.2 GPa, we have analyzed the full widths at half maximum (FWHMs) of the $\nu_3(E_g)$ mode [as it is relatively broad and intense compared to the $\nu_4(E_g)$ mode] at various pressures; see Fig. 4. The experimentally evident discontinuity in the FWHM beyond 18.2 GPa supports the splitting of the $\nu_3(E_g)$ mode and hence indicates that the scheelite-to-fergusonite transition occurs around this pressure. The mode assignment of all the Raman modes in fergusonite-type $ScVO_4$ is done according to our calculations. Table III summarizes the theoretical and experimental Raman mode frequencies and pressure coefficients in fergusonite $ScVO_4$ at 23.3 and 23.4 GPa respectively. The experimental and calculated Raman frequencies and pressure coefficients are in good agreement, thus supporting the observation of the scheelite-to-fergusonite transition.

It should be noted that there is no discontinuity in the volume across the scheelite-to-fergusonite phase transition because it is a displacive second-order phase transition. Therefore, Raman modes do not show a measurable discontinuity across the scheelite-to-fergusonite transformation, as it has been observed in many orthovanadates like YVO_4, $YbVO_4$, and $LuVO_4$.[7,21,25] Figure 2(b) shows the pressure dependence of $ScVO_4$ in the fergusonite phase between 18.2 and 35 GPa. It can be observed that on release of pressure the fergusonite phase was detected until 11 GPa where it transforms back to the scheelite phase. This fact is consistent with the theoretical results, which predict for both transitions a transition pressure smaller (9 GPa) than the experimental value.

To close this section we would like to comment on the fact that XRD studies did not detected the scheelite-to-fergusonite transition. The causes can be multiple. First, the use of different pressure media could strongly affect the structural sequence of ternary oxides like $ScVO_4$.[36] Second, Raman measurements

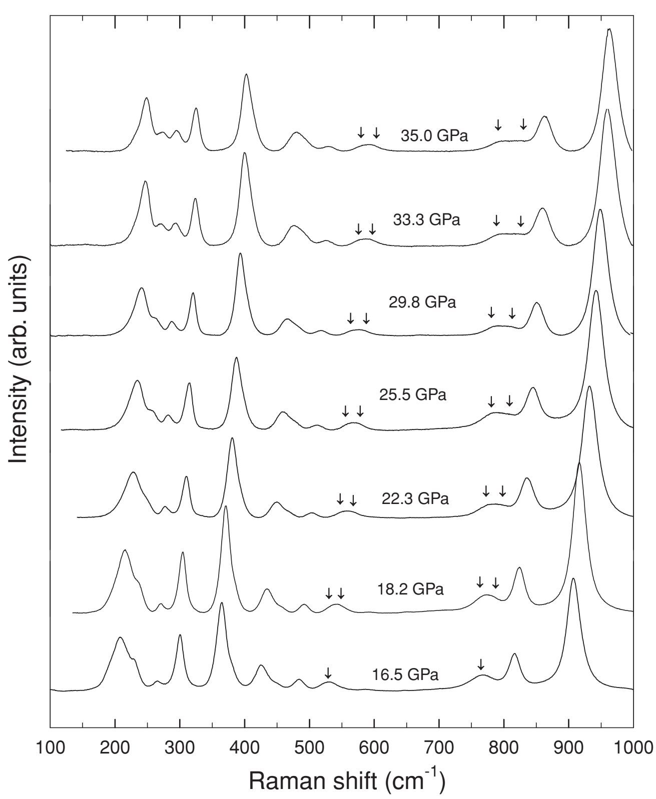

FIG. 3. Raman spectra of the HP fergusonite phase of $ScVO_4$ between 18.2 and 35 GPa. The Raman spectrum of the scheelite phase at 16.5 GPa is also shown for comparison. Arrows show the two modes that exhibit considerable broadening upon compression.

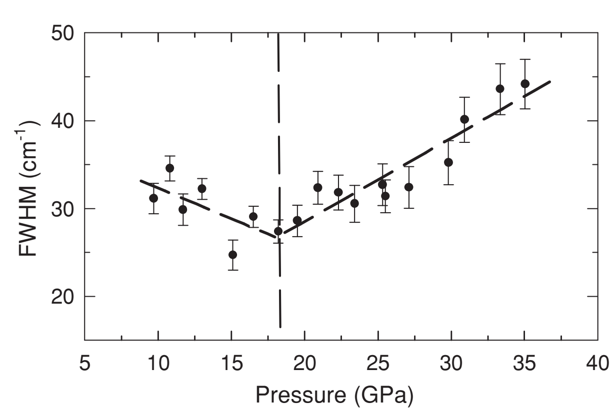

FIG. 4. FWHM of the mode assigned as $\nu_3(E_g)$ in the scheelite phase between 9.7 and 35 GPa. The broadening beyond 18.2 GPa evidences the phase transition.

TABLE III. *Ab initio* calculated frequencies at 23.3 GPa, and experimental frequencies at 23.4 GPa, and pressure coefficients of $ScVO_4$ in the fergusonite phase.

Raman mode symmetry	ω [a] (cm^{-1})	$\frac{d\omega}{dp}$ [a] (cm^{-1}/GPa)	ω [b] (cm^{-1})	$\frac{d\omega}{dp}$ [b] (cm^{-1}/GPa]
B_g	204.3	1.55	–	
A_g	208.7	1.97	228.2	1.83
B_g	237.4	2.19	252.0	2.43
A_g	266.5	1.28	278.6	1.44
B_g	296.2	1.43	311.3	1.27
B_g	302.1	3.69	–	–
A_g	311.8	0.89	–	–
A_g	358.7	1.98	–	–
B_g	379.5	1.48	382.4	1.89
A_g	425.9	2.96	–	–
B_g	441.9	2.09	454.3	2.54
B_g	482.4	2.33	505.4	2.21
B_g	515.4	3.04	557.0	2.54
A_g	536.2	3.44	565.9	2.74
A_g	753.2	1.12	776.0	1.85
B_g	773.7	2.41	800.9	2.46
B_g	836.7	2.05	838.8	2.18
A_g	917.6	2.55	935.3	2.62

[a]Theoretical calculations.
[b]Experimental data.

are more sensitive to subtle phase transitions than XRD.[37] In particular in the case of a second-order transition involving only gradual distortions like the scheelite-to-fergusonite transition. This transition induces important changes in the Raman spectrum (the active modes increase from 13 to 18) but only slight changes in XRD patterns.[38,39] Finally, the broadening induced by pressure in the Bragg peaks[5,40] could mask the onset of the transition. Indeed XRD experiments did not detect the same transition in YVO_4 whereas Raman experiments did.[7] New HP XRD experiments, using a pressure medium like He or Ne, are needed to further investigate the scheelite-to-fergusonite transition in $ScVO_4$ and YVO_4.

V. DISCUSSION

Concerning the structural sequence in zircon-type ABO_4 compounds, it is known that many of them transform to the scheelite phase and then to the fergusonite phase.[3] The zircon-to-scheelite phase transition is a first-order reconstructive phase transition with a probable coexistence of both phases over a wide pressure range,[41] and it has been observed in phosphates,[22,42] chromates,[43,44] vanadates,[5,24–26] germanates,[45] and silicates.[41,46] On the other hand, the scheelite-to-fergusonite transition is a second-order displacive transition involving a smooth transition across the transition pressure[47,48] and it has been reported in tungstates[49,50] and molybdates.[38] In the case of orthovanadates, the complete sequence of structural transformations was previously observed in $LuVO_4$,[25,30] $EuVO_4$,[5] and $YbVO_4$.[21] The second phase transition in $ScVO_4$, namely, from scheelite to fergusonite, has been detected beyond 18.2 GPa in agreement with our total-energy calculation prediction. This pressure is similar to the theoretical pressure for the scheelite-to-fergusonite phase transition in YVO_4 (19 GPa).[7]

Since the scheelite-to-fergusonite transition is ferroelastic displacive in nature,[47] it is expected that there exist an order parameter involving a slight distortion of tetrahedra (tilt or displacement) which is adequate to trigger such transitions. Recently, the presence of a soft $T(B_g)$ mode has been related to the existence of the scheelite-to-fergusonite transition in scheelite-type molybdates and tungstates.[43] We could not detect this $T(B_g)$ mode in the scheelite phase, but our lattice-dynamics calculations predict the softening of the lowest-frequency $T(B_g)$ Raman mode in $ScVO_4$, as was observed in YVO_4,[7] thus suggesting that the scheelite-to-fergusonite transformation could be expected in both compounds. In fact, the scheelite-to-fergusonite phase transition in YVO_4 was predicted near 19 GPa but was not clearly observed until 24 GPa.[7] In this respect, we want to point out that the scheelite-to-fergusonite phase transition has been observed in many rare-earth orthovanadates despite the fact that a soft $T(B_g)$ mode has not been observed in them. At present, we have no explanation for this fact, which implies that the $T(B_g)$ mode softening cannot be regarded as the order parameter involved in the scheelite-to-fergusonite transition in many orthovanadates. In order to clarify this subject, more work is needed.

Zircon-type AVO_4 compounds with a trivalent metal from the lanthanide series show a reduction of the lattice constants and of the A-O and V-O bond distances on decreasing the rare-earth radius. The decrease of the A-O bond length in going from La to Lu is 6% while the V-O bond distance decreases by 0.2%. This small reduction of the V-O bond distance results in an increase of the force constant and consequently leads to a small increase of the symmetric stretching frequency $\nu_1(A_{1g})$ in the zircon phase, as already noted.[51,52] However, it is interesting to observe that the frequency of the symmetric stretching mode $\nu_1(A_g)$ in the scheelite phase remains constant irrespective of the A cation radius. Figure 5(a) shows the stretching Raman mode frequencies in both zircon and scheelite phases for different orthovanadates at ambient pressure as a function of the ionic radius of the A cation.[7,21,22,25,26,53–58] The data corresponding to Figure 5(a) are summarized in Table IV. Note that the described behavior is followed not only for rare-earth orthovanadates, but also for the other members of the orthovanadate family.

The present behavior for the symmetric stretching mode has not been found in other scheelites[31] and it suggests that there is no change in the force constant of the V-O bond in the scheelite phase of orthovanadates despite the reduction of the lattice parameters on decreasing the A cation radius. The dependence of the force constant on the A cation in zircon-type vanadates and the invariability of the force constant in scheelite-type vanadates can be understood in light of the symmetry of the tetragonal zircon and scheelite phases. The scheelite structure is characterized by a setting angle whose value could be between 0 and 45° these are the limit values at which the scheelite structure changes to the more rigid and higher-symmetry zircon structure.[59] Therefore, the scheelite structure can vary its lattice constant when the A cation changes by varying the setting angle but without reducing the V-O bond distance. In this way, the flexible scheelite structure can

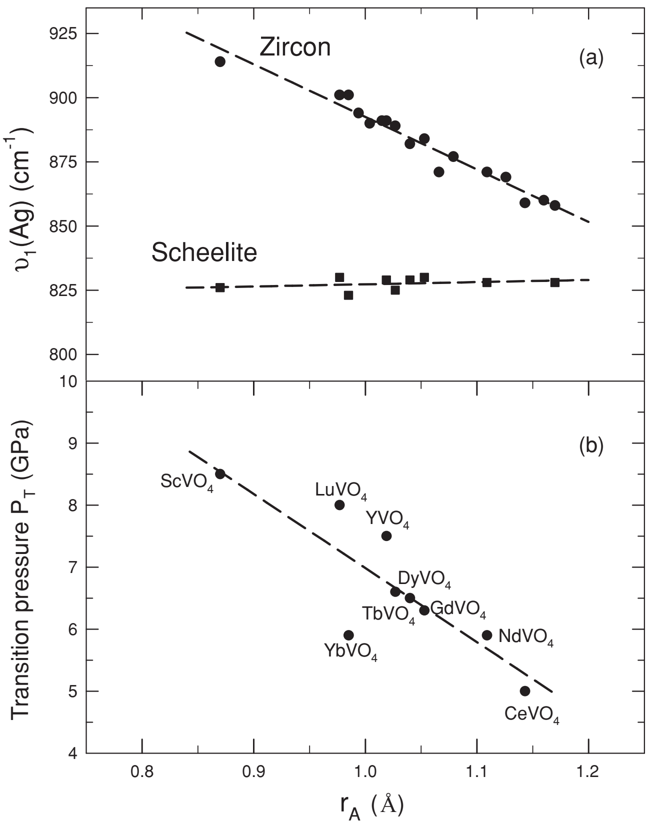

FIG. 5. (a) Experimental symmetric stretching $\nu_1(A_g)$ frequencies in the zircon and scheelite phases for various AVO_4 vanadates as a function of the A cation ionic radius r_A. Circles correspond to zircon phase and squares correspond to scheelite phase. The dashed lines are linear fits of the experimental data. (b) Plot of the zircon-to-scheelite transition pressure for various AVO_4 vanadates as a function of the A cation ionic radius r_A. The dashed line is a linear fit of the experimental data.

accommodate different A cations with decreasing ionic radii by increasing the setting angle without varying the V-O distance. This is not possible in the higher-symmetry zircon phase where the rotation of VO_4 tetrahedra is not allowed and consequently a decrease in the A ionic radius leads to a reduction of the V-O bond distance.

In summary, VO_4 tetrahedra are more symmetric and densely packed in the scheelite phase than in the zircon phase due to the tetrahedral tilting available in the less symmetric tetragonal scheelite phase compared to the rigid zircon phase. Consequently, the change of A cation radius in scheelite orthovanadates does not result in a change in V-O bond distance nor in a change of the V-O force constant but in a different setting angle for each compound. In contrast, the rigid VO_4 tetrahedra of the zircon phase cannot rotate and must change the V-O bond distance. Consequently, the V-O force constant depends upon the A cation radius.

Furthermore, we have noted a dependence of the zircon-to-scheelite phase transition pressure in AVO_4 compounds on the A ionic radius [see Fig. 5(b)]. Table V summarizes the zircon-to-scheelite transition pressures (obtained from Raman experiments) as a function of the ionic radius of the A cation. The higher the ionic radius is, the lower the phase-transition pressure. This result is directly related to the position of the orthovanadates in the Bastide diagram[3] and is in good agreement with the observation that orthovanadates with large A ionic radii can also be crystallized either in the scheelite ($BiVO_4$)[60] or in the monazite ($LaVO_4$)[61] phase. Summarizing, these results indicate that the zircon phase is more stable in compounds with a small ionic radius of the A cation. According to this conclusion, $ErVO_4$ and $HoVO_4$ are predicted to undergo phase transitions near 7 GPa, $EuVO_4$ and $SmVO_4$ at 6 GPa, and $PrVO_4$ at 5 GPa. The prediction made for $EuVO_4$ is consistent with the results obtained in XRD measurements,[5] where the transition pressure is slightly larger, as found in other vanadates when XRD and Raman studies are compared.

Finally, we should mention that according to our estimations of bulk moduli in scheelite-type compounds,[62] the compressibility of scheelite-type AVO_4 compounds is directly

TABLE IV. Symmetric stretching frequency at ambient pressure ω_0 of the $\nu_1(A_g)$ mode for various AVO_4 vanadates in both zircon and scheelite phases as a function of their A ionic radius (Shannon radius) r_A.

Compound	r_A (Å)	w_0 (cm^{-1}) [a]	w_0 (cm^{-1}) [b]	References
$ScVO_4$	0.87	914	826	This work
$LuVO_4$	0.977	901	830	25
$YbVO_4$	0.985	901	823	21, 22
$TmVO_4$	0.994	894		22
$ErVO_4$	1.004	890		22
$HoVO_4$	1.015	891		22
YVO_4	1.019	891	829	7
$DyVO_4$	1.027	889	825	26
$TbVO_4$	1.04	882	829	26
$GdVO_4$	1.053	884	830	54, 55
$EuVO_4$	1.066	871		56
$SmVO_4$	1.079	877		22
$NdVO_4$	1.109	871	828	53
$PrVO_4$	1.126	869		22
$CeVO_4$	1.143	859	826	22, 53
$LaVO_4$	1.16	860		22
$BiVO_4$	1.17	858	828	56, 58

[a]Zircon phase.
[b]Scheelite phase.

TABLE V. Zircon-to-scheelite phase transition pressure P_T for various AVO_4 vanadates as a function of the A cation ionic radius (Shannon radius) r_A.

Compound	r_A (Å)	P_T (GPa)	References
$ScVO_4$	0.87	8.5	This work
$LuVO_4$	0.977	8.0	25
$YbVO_4$	0.985	5.9	21
YVO_4	0.95	7.5	7
$DyVO_4$	1.027	6.6	26
$TbVO_4$	1.04	6.5	26
$GdVO_4$	1.053	6.3	54
$NdVO_4$	1.109	5.9	53
$CeVO_4$	1.143	5.0	53

related to the compressibility of the AO_8 polyhedra due to the rather incompressible VO_4 tetrahedra. Therefore, $ScVO_4$ should have the least volume among the orthovanadates due to the small ionic radius of Sc and a very high bulk modulus due to the high incompressibility of the ScO_8 polyhedra. Recent HP XRD measurements support our arguments.[5]

VI. CONCLUSIONS

Our combined experimental and theoretical study of scandium orthovanadate up to 35 GPa suggests that the low-pressure zircon phase undergoes an irreversible zircon-to-scheelite phase transition above 8.2 GPa. Beyond 18.2 GPa the $\nu_4(E_g)$ and $\nu_3(E_g)$ scheelite modes show a gradual splitting, indicating the onset of the scheelite-to-fergusonite phase transition. On release of pressure the fergusonite phase was detected down to 11 GPa. Below 11 GPa the sample retains the metastable scheelite phase even at ambient pressure. The symmetries of the Raman modes in the zircon, scheelite, and fergusonite phases of $ScVO_4$ have been assigned by use of lattice-dynamics calculations. In general, a good agreement is found between our experimental and theoretical data.

We have evidenced and discussed a notable dependence of the symmetric stretching mode frequencies on the radius of the A cation in AVO_4 compounds in the zircon phase, unlike in the scheelite phase. Similarly, a considerable dependence of the zircon-to-scheelite transition pressure and of the bulk compressibility of the zircon phase on the A cation ionic radius is evidenced. Additionally, we have noted a lack of a soft mode behavior in some scheelite-type rare-earth orthovanadates, unlike $ScVO_4$ and YVO_4. All these results deserve a deeper analysis of the HP behavior of orthovanadates that we hope to stimulate with this work.

ACKNOWLEDGMENTS

We acknowledge the financial support of the Spanish MCYT under Grants No. MAT2007-65990-C03-01/03, No. MAT2010-21270-C04-01/03/04, and No. CSD2007-00045, and the computation time provided by the Red Española de Supercomputación and the supercomputer Atlante. F.J.M. acknowledges also financial support from "Vicerrectorado de Innovación y Desarrollo de la UPV" (No. PAID-05-2009 through Project No. UPV2010-0096). Some of the authors are members of the MALTA Consolider Team.

*Corresponding author: daniel.errandonea@uv.es

[1] S. P. Shafi, M. W. Kotyk, L. M. D. Cranswick, V. K. Michaelis, S. Kroeker, and M. Bieringer, Inorg. Chem. **48**, 10553 (2009), and references therein.
[2] D. F. Mullica, E. L. Sappenifield, M. M. Abraham, B. C. Chakoumakos, and L. A. Boatner, Inorg. Chim. Acta **248**, 85 (1996).
[3] D. Errandonea and F. J. Manjón, Prog. Mater. Sci. **53**, 711 (2008).
[4] T. Aldred, Acta Crystallogr. Sect. B **40**, 569 (1984).
[5] D. Errandonea, R. Lacomba-Perales, J. Ruiz-Fuertes, A. Segura, S. N. Achary, and A. K. Tyagi, Phys. Rev. B **79**, 184104 (2009).
[6] J. López-Solano, P. Rodríguez-Hernández, and A. Muñoz, High Press. Res. **29**, 582 (2009).
[7] F. J. Manjón, P. Rodríguez-Hernández, A. Muñoz, A. H. Romero, and D. Errandonea, Phys. Rev. B **81**, 075202 (2010).
[8] X. Wang, I. Loa, K. Syassen, M. Hanfland, and B. Ferrand, Phys. Rev. B **70**, 064109 (2004).
[9] S. Klotz, L. Paumier, G. Le Marchand, and P. Munsch, J. Phys. D **42**, 075413 (2009).
[10] D. Errandonea, Y. Meng, M. Somayazulu, and D. Häusermann, Physica B **355**, 116 (2005).
[11] H. K. Mao, J. Xu, and P. M. Bell, J. Geophys. Res. **91**, 4673 (1986).
[12] G. Kresse and J. Furthmüller, Phys. Rev. B **54**, 11169 (1996).
[13] G. Kresse and D. Joubert, Phys. Rev. B **59**, 1758 (1999).
[14] P. E. Blöchl, Phys. Rev. B **50**, 17953 (1994).
[15] G. Kresse and D. Joubert, Phys. Rev. B **59**, 1758 (1999).
[16] J. P. Perdew, S. Burke, and M. Ernzerhof, Phys. Rev. Lett. **77**, 3865 (1996).
[17] A. Mujica, A. Rubio, A. Muñoz, and R. J. Needs, Rev. Mod. Phys. **79**, 863 (2003).
[18] K. Parlinski, computer code PHONON, [http://wolf.ifj.edu.pl/phonon].
[19] G. Herzberg, *Molecular Spectra and Molecular Structure II: Infra-Red and Raman Spectra* (Van Nostrand, New York, 1945).
[20] I. Guedes, Y. Hirano, M. Grimsditch, N. Wakabayashi, C. K. Loong, and L. A. Boatner, J. Appl. Phys. **90**, 1843 (2001).
[21] A. B. Garg, R. Rao, T. Sakuntala, B. N. Wani, and V. Vijayakumar, J. Appl. Phys. **106**, 063513 (2009).
[22] C. C. Santos, E. N. Silva, A. P. Ayala, and I. Guedes, J. Appl. Phys. **101**, 053511 (2001).
[23] F. X. Zhang, J. W. Wang, M. Lang, J. M. Zhang, and R. C. Ewing, Phys. Rev. B **80**, 184114 (2009).
[24] J. A. Tossell, J. Am. Chem. Soc. **97**, 4840 (1975).
[25] R. Rao, A. B. Garg, T. Sakuntala, S. N. Achary, and A. K. Tyagi, J. Solid. State Chem. **182**, 1879 (2009).
[26] S. J. Duclos, A. Jayaraman, G. P. Espinosa, A. S. Cooper, and R. G. Maines, J. Phys. Chem. Solids **50**, 769 (1989).
[27] M. B. Smirnov, A. P. Mirgorodsky, V. Yu. Kazimirov, and R. Guinebretière, Phys. Rev. B **78**, 094109 (2008).
[28] M. Flórez, J. Contreras-García, J. M. Recio, and M. Marquez, Phys. Rev. B **79**, 104101 (2009).
[29] D. L. Rousseau, R. P. Baumann, and S. P. Porto, J. Raman Spectrosc. **10**, 253 (1981).
[30] R. Mittal, A. B. Garg, V. Vijaykumar, S. N. Achary, A. K. Tyagi, B. K. Godwal, E. Busetto, A. Lausi, and S. L. Chaplot, J. Phys. Condens. Matter **20**, 075223 (2008).
[31] F. J. Manjón, D. Errandonea, N. Garro, J. Pellicer-Porres, P. Rodríguez Hernández, S. Radescu, J. López-Solano, A. Mujica, and A. Muñoz, Phys. Rev. B **74**, 144111 (2006).
[32] F. J. Manjón, D. Errandonea, N. Garro, J. Pellicer-Porres, J. López-Solano, P. Rodríguez Hernández, S. Radescu, A. Mujica, and A. Muñoz, Phys. Rev. B **74**, 144112 (2006).
[33] V. Panchal, N. Garg, and S. M. Sharma, J. Phys. Condens. Matter **18**, 3917 (2008).
[34] F. D. Hardcastle and I. E. Wachs, J. Phys. Chem. **95**, 5031 (1991).
[35] I. D. Brown and K. K. Wu, Acta Crystallogr. Sect. B **32**, 1957 (1976).

[36]R. Lacomba-Perales, D. Martínez-García, D. Errandonea, Y. Le Godec, J. Phillipe, G. Le Marchand, J. C. Chervin, A. Polian, A. Muñoz, and J. Lopez-Solano, Phys. Rev. B **80**, 144117 (2010).

[37]O. Tschauner, D. Errandonea, and G. Serghiou, Physica B **371**, 88 (2006).

[38]D. Errandonea, R. S. Kumar, X. Ma, and C. Y. Tu, J. Solid State Chem. **181**, 355 (2008).

[39]D. Errandonea, D. Santamaria-Perez, V. Grover, S. N. Achary, and A. K. Tyagi, J. Appl. Phys. **108**, 073518 (2010).

[40]D. Errandonea, D. Santamaria-Perez, T. Bondarenko, and O. Khyzhun, Mater. Res. Bull. **45**, 1732 (2010).

[41]M. Marqués, M. Florez, J. M. Recio, L. Gerward, and J. Staun Olsen, Phys. Rev. B **74**, 014104 (2006).

[42]R. Lacomba-Perales, D. Errandonea, Y. Meng, and M. Bettinelli, Phys. Rev. B **81**, 064113 (2010).

[43]Y. W. Long, W. W. Zhang, L. X. Yang, Y. Yu, R. C. Yu, S. Ding, Y. L. Liu, and C. Q. Jin, Appl. Phys. Lett. **87**, 181901 (2005).

[44]Y. W. Long, L. X. Yang, Y. Yu, F. Y. Li, R. C. Yu, S. Ding, Y. L. Liu, and C. Q. Jin, Phys. Rev. B **74**, 054110 (2006).

[45]D. Errandonea, R. S. Kumar, L. Gracia, A. Beltrán, S. N. Achary, and A. K. Tyagi, Phys. Rev. B **80**, 094101 (2009).

[46]L. Gracia, A. Beltrán, and D. Errandonea, Phys. Rev. B **80**, 094105 (2009).

[47]D. Errandonea, Europhys. Lett. **77**, 56001 (2007).

[48]D. Errandonea and F. J. Manjón, Mater. Res. Bull. **44**, 807 (2009).

[49]D. Errandonea, J. Pellicer-Porres, F. J. Manjón, A. Segura, Ch. Ferrer-Roca, R. S. Kumar, O. Tschauner, P. Rodríguez Hernández, J. López-Solano, S. Radescu, A. Mujica, A. Muñoz, and G. Aquilanti, Phys. Rev. B **72**, 174106 (2005).

[50]D. Errandonea, Phys. Status Solidi B **242**, R125 (2005).

[51]G. M. Begun, G. W. Beall, L. A. Boatner, and W. J. Gregor, J. Raman Spectrosc. **11**, 273 (1981).

[52]R. Podor, Eur. J. Mineral. **7**, 1353 (1995).

[53]V. Panchal *et al.* (unpublished).

[54]C. C Zhang, Z. M. Zhang, R. C. Dai, Z. P. Wang, J. W. Zhang, and Z. J. Ding, J. Phys. Chem. C **114**, 18279 (2010).

[55]Y. K. Voronko, A. A. Sobol, V. E. Shukshin, A. I. Zagumennyi, Y. D. Zavartsev, and S. A. Kutovoi, Phys. Solid State **51**, 1886 (2009).

[56]V. E. J. Baran, M. E. Escobar, L. L. Fournier, and R. R. Filgueira, Z. Anorg. Allg. Chem. **472**, 193 (1981).

[57]R. L. Frost, D. A. Henry, M. L. Weier, and W. Martens, J. Raman Spectrosc. **37**, 722 (2006).

[58]J. L. Blin, A. L. Rubbens, F. Wallart, and J. P. Wignacourt, J. Mater. Chem. **6**, 385 (1996).

[59]F. J. Manjón, D. Errandonea, J. López-Solano, P. Rodríguez Hernández, and A. Muñoz, J. Appl. Phys. **105**, 094321 (2009).

[60]S. Tokunaga, H. Kato, and A. Kudo, Chem. Mater. **13**, 4624 (2001).

[61]C. E. Rice and W. R. Robinson, Acta Crystallogr. Sect. B **32**, 2232 (1976).

[62]D. Errandonea, F. J. Manjón, M. Somayazulu, and D. Häusermann, J. Solid State Chem. **177**, 1087 (2004).